

## Generation of second-harmonic Ince-Gaussian beams

Meng-Ying Wang, Jie Tang, Hui-Jun Wang, Yang Ming, Yong Zhang, Guo-Xin Cui, and Yan-Qing Lu

Citation: *Appl. Phys. Lett.* **113**, 081105 (2018); doi: 10.1063/1.5041986

View online: <https://doi.org/10.1063/1.5041986>

View Table of Contents: <http://aip.scitation.org/toc/apl/113/8>

Published by the [American Institute of Physics](#)

---

---

**AIP** | Conference Proceedings

Get **30% off** all  
print proceedings!

Enter Promotion Code **PDF30** at checkout



## Generation of second-harmonic Ince-Gaussian beams

Meng-Ying Wang,<sup>1,a)</sup> Jie Tang,<sup>1,a)</sup> Hui-Jun Wang,<sup>2</sup> Yang Ming,<sup>1</sup> Yong Zhang,<sup>1</sup>  
 Guo-Xin Cui,<sup>1,b)</sup> and Yan-Qing Lu<sup>1</sup>

<sup>1</sup>National Laboratory of Solid State Microstructures, College of Engineering and Applied Sciences,  
 Nanjing University, Nanjing 210093, China

<sup>2</sup>Department of Physics, Nanjing University, Nanjing 210093, China

(Received 28 May 2018; accepted 8 August 2018; published online 23 August 2018)

As a continuous transition between the Hermite-Gaussian and Laguerre-Gaussian beams, the Ince-Gaussian beams form a family of exact orthogonal solutions of the free-space paraxial wave equation in elliptic coordinates. Ince-Gaussian beams have multiple transverse mode patterns, which make them unique in terms of application in the fields of bioengineering, particle manipulation, and quantum entanglement. Here, based on binary nonlinear computer-generated holograms with a domain structure (realized via electric field poling at room temperature), we generate a second-harmonic Ince-Gaussian beam pumped with a fundamental Gaussian beam. In this process, the transverse part of the phase-matching condition is satisfied, which is called the Raman-Nath-type nonlinear diffraction. Both frequency conversion and beam shaping can be realized simultaneously, thereby offering the advantage of integration of both functions into a single device. *Published by AIP Publishing.* <https://doi.org/10.1063/1.5041986>

In recent years, beam shaping based on the technology of computer-generated holograms (CGHs) has attracted considerable attention in the field of nonlinear optics.<sup>1</sup> Originally, one-dimensional (1D) beam shaping was developed, followed by two-dimensional (2D) beam shaping. In the field of nonlinear optics, 1D beam shaping was proposed by Imeshev *et al.*<sup>2</sup> The process involved changing the optical interaction length to generate a flat-top beam at the output of a crystal surface. This approach can be used for the arbitrary amplitude modulation of a 1D beam. In 2002, Kurtz *et al.*<sup>3</sup> realized a modulated output beam phase with a linear phase array and lens. Further, in 2007, Ellenbogen *et al.*<sup>4</sup> observed a self-accelerating beam with a cubic phase, which is called an Airy beam.<sup>5</sup> Subsequently, Bahabad and Arie<sup>6</sup> proposed a method to produce frequency converted vortex beams with a fork grating in quadratic nonlinear crystals. Another study in 2015 summarized the method of generating arbitrary 2D beams based on nonlinear optical computer holographic theory.<sup>7</sup> In this context, beam shaping and nonlinear frequency conversion are expected to open up more possibilities in the field of nonlinear optics. For example, Ming *et al.* investigated the wavefront engineering of photon pairs generated through spontaneous parametric down-conversion in lithium niobate (LN)-based nonlinear photonics.<sup>8</sup> Further, the entanglement of photons with complex spatial structures in the Hermite-Laguerre-Gaussian mode was proposed, which can be used in quantum entanglement.<sup>9</sup> The shape and direction of the generated beam depend on the phase-matching conditions.<sup>10</sup> For 2D beam shaping, only the transverse part of the phase-matching condition requires to be satisfied.<sup>11</sup>

In this study, we generate a second harmonic (SH) Ince-Gaussian beam (IGB) based on binary nonlinear CGHs using quadratic nonlinear crystals. In this context, in 2004, Bandres and Gutiérrez-Vega<sup>12</sup> proposed a family of exact

orthogonal solutions of the free-space paraxial wave equation (PWE) in elliptic coordinates, named the IG modes, which constitute the exact and continuous transition modes between the Hermite-Gaussian (HG) and Laguerre-Gaussian (LG) modes.<sup>12</sup> In addition, IG beams are modes of stable resonators.<sup>13,14</sup> The elliptical profiles of the IG modes are diversified, and the helical IG modes<sup>15</sup> carry orbital angular momentum, which makes IG modes widely applicable in areas such as biological medicine,<sup>16</sup> particle manipulation,<sup>17</sup> and quantum entanglement.<sup>18</sup> One key difference of this work in comparison with the previous one is that we pushed the sample thickness to be 10-times thinner. It is only about 45  $\mu\text{m}$  and the size is as big as  $\sim 1\text{ cm}^2$ . This is very important not only on finer pattern accuracy and better domain quality, but also the more effective SH efficiency. In the process, only the transverse part of the phase-matching is fulfilled, which is called nonlinear Raman-Nath diffraction.<sup>11</sup> In our experiment, the coherence length<sup>19</sup> is less than the thickness of LN thin film and consequently the field amplitude of SH oscillates periodically with the distance. Therefore, a bulk LN is not helpful. In addition, the LN thin film still has advantages in the sample preparation and integration. It is easier to carry out the domain inversion process at room temperature because of its high coercive field ( $\sim 21\text{ kV/mm}$ ). Moreover, the domain structure with a high resolution can be realized by using the LN thin film, which is beneficial to generate a structure laser beam with complex intensity distribution. The domain structures are consistent on both  $\pm c$  sides of samples, which avoids the appearance of needle-like or wedge-like ferroelectric domain,<sup>20</sup> so the quality of the SH IGBs is better.

The most commonly used method of 2D beam shaping is CGH. The amplitude and phase of the object beam is stored in the holograms. When the reference beam illuminates the holograms, the desired beam appears in the far field. As early as 1967, Burch<sup>21</sup> used Eq. (1) to describe the amplitude transmittance of holograms

<sup>a)</sup>M.-Y. Wang and J. Tang contributed equally to this work.

<sup>b)</sup>Electronic mail: cuiguoxin@nju.edu.cn.

$$t(x, y) = 0.5 \{ 1 + A(x, y) \cos(2\pi f_{carrier} x - \varphi(x, y)) \}. \quad (1)$$

Here,  $f_{carrier}$  denotes the carrier frequency, and  $A(x, y)$  and  $\varphi(x, y)$  the amplitude and phase of the Fourier transform (FT) of the desired beam in the first diffraction order, respectively. As the quadratic susceptibility of quadratic nonlinear crystals is either positive or negative, Eq. (1) needs to be transformed into the binary form. In 1979, Lee<sup>22</sup> proposed the concept of boundary CGHs, in which the amplitude transmittance can be expressed as

$$t(x, y) = \begin{cases} 1, & \cos(2\pi f_{carrier} x - \varphi(x, y)) - \cos(\pi q(x, y)) \geq 0 \\ 0, & \text{else.} \end{cases} \quad (2)$$

Here,  $q(x, y)$  satisfies  $\sin(\pi q(x, y)) = A(x, y)$ ,<sup>22</sup> and therefore, the polarization pattern has the following expression:

$$d(x, y) = d_{ij} \text{Sign}(\cos(2\pi f_{carrier} x - \varphi(x, y)) - \cos(\pi q(x, y))), \quad (3)$$

where  $d_{ij}$  represents an element of the quadratic susceptibility tensor. Equation (4) represents the Fourier series decomposition of Eq. (2), which indicates why we can realize the desired beam in the first diffraction order ( $m = 1$ )

$$t(x, y) = \sum_{m=-\infty}^{+\infty} \left\{ \frac{\sin(m\pi q(x, y))}{m\pi} \times \exp[im(2\pi f_{carrier} x - \varphi(x, y))] \right\}. \quad (4)$$

Based on this method, we can obtain holograms encoded with the information of the IGB. The transverse spatial distribution of the IG mode at  $z = 0$  is<sup>13</sup>

$$IG_{p,m}^e(r, \varepsilon) = C \times C_p^m(i\xi, \varepsilon) C_p^m(\eta, \varepsilon) \exp\left(-\frac{r^2}{\omega_0^2}\right), \quad (5)$$

$$IG_{p,m}^o(r, \varepsilon) = S \times S_p^m(i\xi, \varepsilon) S_p^m(\eta, \varepsilon) \exp\left(-\frac{r^2}{\omega_0^2}\right).$$

In the above equations, the superscripts  $e$  and  $o$  refer to the even modes and odd modes, respectively,  $C$  and  $S$  denote the normalization constants, and  $C_p^m$  and  $S_p^m$  denote even and odd Ince polynomials of order  $p$  and degree  $m$ , respectively. We note here that parameters  $p$  and  $m$  always have the same parity. They are related as  $0 \leq m \leq p$  for even functions and  $1 \leq m \leq p$  for odd functions. Further,  $\varepsilon$  denotes the ellipticity parameter,  $(\xi, \eta)$  the elliptic coordinates, and  $\omega_0$  the beam width at  $z = 0$ . Since the FTs of the IG modes yield the unchanged IG modes themselves, the holograms can be directly calculated by means of Eqs. (3) and (5).

We fabricated a pattern-poled LN crystal film via electric field poling, wherein a strong applied electric field was used to invert the internal polarization vector.<sup>23</sup> The process of preparing the pattern electrode is shown in Fig. 1, which mainly includes fixing the sample with petrolin, coating glue, maskless lithography, deposition, lift-off, and dismantling the sample.

Finally, the domain inverted structure was obtained by applying a high voltage to the pattern electrode at room temperature. The poling process is shown in Fig. 2. The use of NaCl solution enables the formation of an ohmic contact between the -C surface of the LN crystal film and the ITO glass substrate. We next applied a pulse bias voltage (duty cycle = 50%; frequency = 1 Hz; and duration = 10 pulses) slightly larger than the coercive electric field of the LN crystal film. In our experiment, the applied voltage was about 1060 V. Next, we removed the metal pattern electrode with Cr-corrosive liquid. Here, we remark that our approach can

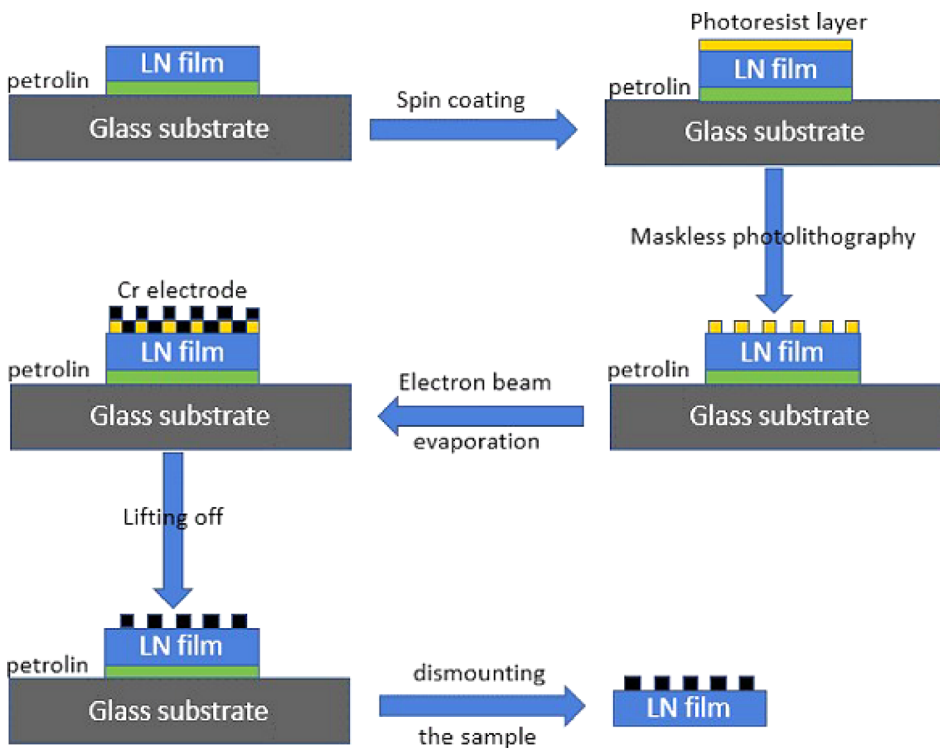


FIG. 1. Schematic of sample preparation.

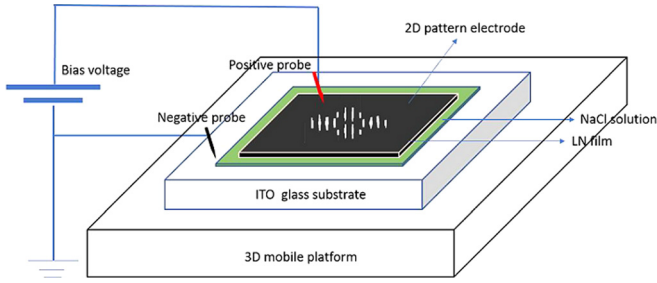


FIG. 2. Schematic of poled device.

be easily followed at room temperature. Moreover, the domain structure is uniform, perforated, and stable.

Figure 3 compares the calculated and fabricated poled structures for several different IG modes. Figure 3(b) was measured by CCD when fundamental wave illuminates on the surface of samples. The size of the patterns is about  $0.2 \times 0.2 \text{ mm}^2$ . The resolution of the domain structures is approximately  $2 \mu\text{m}$ . The high quality of the samples can be inferred from the figure.

In our experiment, the fundamental wave was obtained from a Ti:sapphire femtosecond-pulsed laser (pulse width: 140 fs; repetition rate: 80 MHz) operating at a wavelength of 900 nm. The fundamental wave was focused by a lens ( $f = 150 \text{ mm}$ ) at the crystal. Our experimental setup is shown in Fig. 4. The SH IGB was observed in the first diffraction order (+1 and -1). The carrier frequency was chosen to be  $0.07 \mu\text{m}^{-1}$ , and hence, the angle of the first diffraction order was computed as  $\sin(\vartheta) = \lambda_{SH} f_{carrier}$  ( $\sim 31.5 \text{ mrad}$ ), where  $\lambda_{SH}$  denotes the SH wavelength.<sup>11</sup> The damage threshold<sup>24</sup> of crystal is an important parameter of the device. The

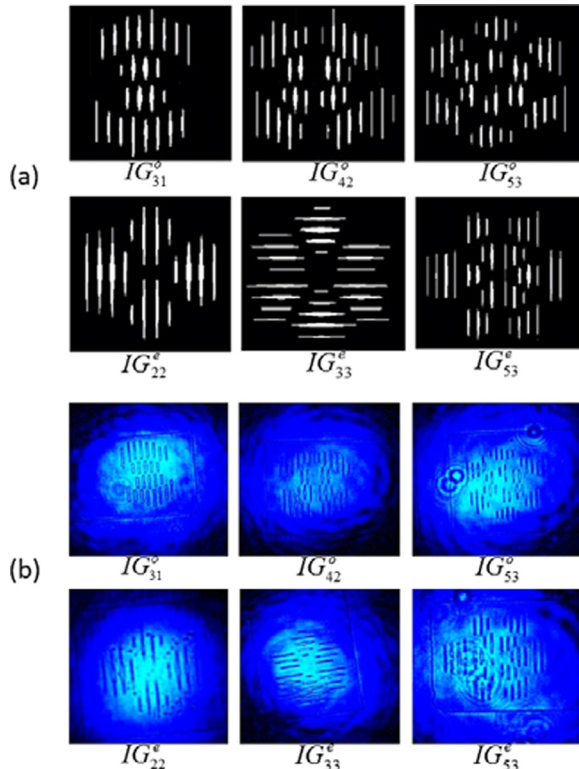
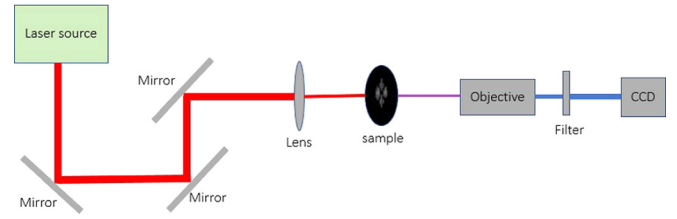
FIG. 3. Comparison between (a) calculated and (b) fabricated poling patterns for  $IG_{31}^o$ ,  $IG_{42}^o$ ,  $IG_{53}^o$ ,  $IG_{22}^e$ ,  $IG_{33}^e$ , and  $IG_{53}^e$  modes.

FIG. 4. Experiment setup utilized to generate second-harmonic Ince-Gaussian beam (SH IGB).

damage threshold of congruent LN crystal is approximately  $14.3 \text{ kW/cm}^2$ ,<sup>25</sup> which is big enough to be ignored in our experiment. Figure 5 compares the theoretical and measured profiles of several different IG modes in the first diffraction order. The results indicate that the experimental results are in conformity with the theoretical predictions.

In addition to the IG mode, the HG and LG modes also form exact orthogonal solutions of the PWE in Cartesian and polar coordinates, respectively. The IG mode can be considered as a continuous transition between the HG and LG modes. When  $\varepsilon \rightarrow \infty$ , the  $IG_{p,m}^{e,o}$  mode becomes the  $HG_{n_x, n_y}$  mode, and the conditions  $n_x = m$ ,  $n_y = p - m$  are satisfied for even IGBs, while the conditions  $n_x = m - 1$ ,  $n_y = p - m - 1$  are satisfied for odd IGBs.<sup>12</sup> When  $\varepsilon \rightarrow 0$ , the  $IG_{p,m}^{e,o}$  mode becomes the  $LG_{n,l}$  mode, which satisfies  $l = m$ ,  $n = (p - m)/2$ .<sup>12</sup> Parameter  $l$  is called the topological charge. Figure 6 attempts to further clearly elucidate the conversion relations between the three modes. From Fig. 6, we note that  $HG_{52}$  is similar to  $IG_{73}^o$ , and  $HG_{43}$  is similar to  $IG_{73}^e$  when  $\varepsilon \rightarrow \infty$ . Further,  $LG_{23}$  is similar to  $IG_{73}^o$  and  $IG_{73}^e$  when  $\varepsilon \rightarrow 0$ .

Similarly, we next generated the SH  $HG_{11}$  and  $LG_{11}$  modes; Fig. 7 compares the theoretical and measured profiles in the first diffraction order. Again, the experimental results

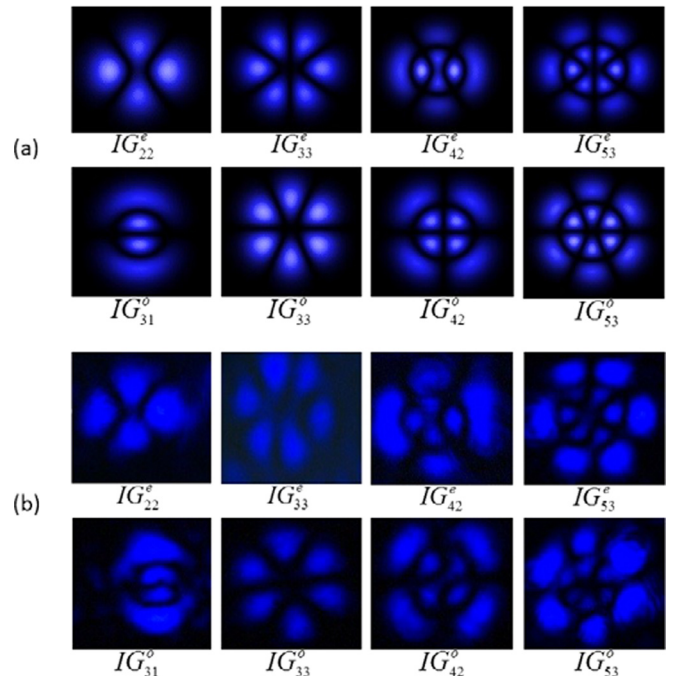


FIG. 5. Comparison of (a) theoretical and (b) measured Ince-Gaussian beams (IGBs) in the first diffraction order.

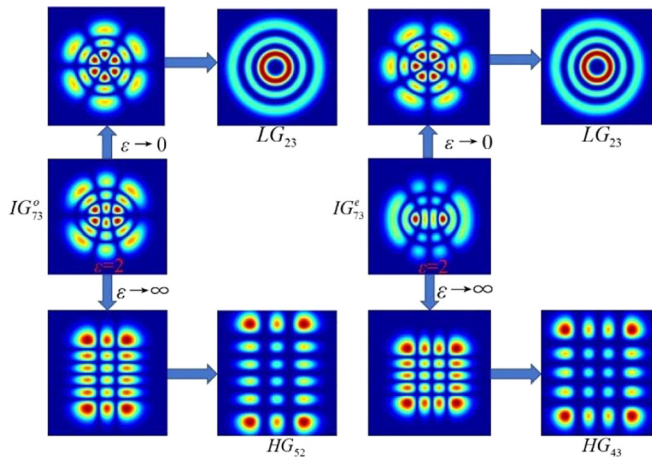


FIG. 6. Schematic illustration of conversion relations between three modes.

agree with the theoretical calculations. The LG mode corresponds to a vortex beam, which has a phase singularity and carries orbital angular momentum  $lh$ .<sup>26</sup> Various applications have been found for vortex beams, for example, in optical tweezers<sup>27</sup> and actuators for microelectromechanical systems,<sup>28</sup> multi-dimensional quantum entanglement,<sup>29</sup> and extrasolar planet detection.<sup>30</sup> As the continuous transition between HG and LG, the IG mode has similar applications.

We examined both the total SH generation and the power of the first diffraction order. A different fraction of the total SH power is diffracted to the first diffraction order in each structure. The percentages of desired SHBs are 19.5%, 13.2%, 24.2%, and 9.5%, corresponding to  $IG_{53}^o$ ,  $IG_{42}^e$ ,  $LG_{11}$  and  $HG_{11}$ . The predicted conversion efficiency is  $8.73 \times 10^{-11} \%W^{-1}$ , and the measured one is approximately  $5.21 \times 10^{-11} \%W^{-1}$ , which is similar to the previous work on generating SH LG and HG modes.<sup>31</sup> The main reason for low efficiency is that the full vectorial phase-matching condition is not fulfilled. Under this condition, the intensity of SH at the exit plane of the nonlinear medium is given by

Ref. 32. The wavevector mismatch  $\Delta k$  is about  $1.88 \mu\text{m}^{-1}$  in our experiment, so the coherence length  $\frac{\pi}{\Delta k}$  for 900 nm FW is about  $1.67 \mu\text{m}$ . The coherence length is less than the thickness of LN thin film, and consequently, the field amplitude of SH oscillates periodically with distance. Therefore, a bulk LN is not helpful. An improvement of the efficiency can be achieved by working with the Saltiel<sup>33</sup> phase-matching scheme or the Saltiel<sup>11</sup> phase-matching scheme, which will require submicron patterning of the nonlinear crystal.

Laser beam quality<sup>34</sup> is an important issue of the laser. The most commonly used to evaluate the quality of laser beam is  $M^2$  factor.<sup>35</sup> However, there are limitations in using the  $M^2$  factor to evaluate the beam quality. It is not suitable for evaluation of structure laser beam with complex intensity distribution.<sup>36</sup> Therefore, we would measure the far field divergence angle<sup>37</sup> of the generated IG mode and compared it with the theoretical result. This could still give some information of the beam quality after direct observation of beam images. At a distance of 30 cm from the exit surface of the sample, the IGBs were photographed and the diameters were measured every 1 mm. The average divergence angle is 3.731 mrad, which is similar to the theoretical result (approximately 3.23 mrad). The deviation mainly comes from the measurement and fabrication of samples. Besides  $IG_{53}^o$ , the divergence angles of  $IG_{42}^e$ ,  $LG_{11}$ , and  $HG_{11}$  were measured. They are 2.902, 3.493, and 1.593 mrad, respectively, which is consistent with the theoretical results.

From Figs. 3, 5, and 7, we can observe some deviations between the experimental results and theoretical calculations. These deviations can be mainly attributed to the following reasons: (i) the applied voltage (about 1060 V) is not the most appropriate voltage for reversing the domain structure, which results in deviations of the domain structures from the computed holograms. (ii) The sample surfaces are not sufficiently smooth and clean. (iii) The fundamental wave does not illuminate the center of the holograms. We believe that a better shaping performance can be achieved via improving on the above defects, for example, preparing finer domain structures via choosing suitable voltages, improved sample polishing and cleaning, and adjusting the fundamental wave to precisely illuminate the center of the holograms.

In conclusion, we fabricated pattern-poled LN crystal films as holograms via electric field poling. Based on binary nonlinear CGHs, we generated second-harmonic Ince-Gaussian beams with a fundamental pump Gaussian beam. Our approach realizes frequency conversion and beam shaping simultaneously. The introduction of holographic techniques can generate arbitrary shapes of beams flexibly and avoid the use of additional elements such as lenses and splitters, which is advantageous in terms of integration of both features in a single device. A thinner film is still more effective in terms of overall conversion efficiency versus sample thickness and makes it easier to carry out the domain inversion process. The generated second-harmonic IGBs can be widely used in bioengineering, particle manipulation, and quantum entanglement.

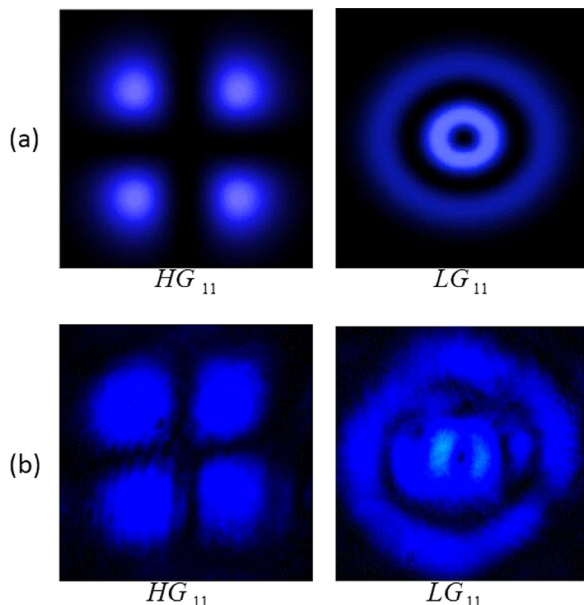


FIG. 7. Comparison between (a) theoretical and (b) measured profiles of  $HG_{11}$  and  $LG_{11}$  in the first diffraction order.

This work was supported by National Key R&D Program of China (2017YFA0303701), National Natural

Science Foundation of China (NSFC) (Grant Nos. 61490712, 11604144, and 11704182), and Fundamental Research Funds for the Central Universities (14380001).

We thank the microfabrication center at the National Laboratory of Solid State Microstructures, Nanjing University, for their technical support in manufacturing the pattern-poled LN crystal films.

- <sup>1</sup>V. Berger, "Nonlinear photonic crystals," *Phys. Rev. Lett.* **81**, 4136 (1998).
- <sup>2</sup>G. Imeshev, M. Proctor, and M. M. Fejer, "Lateral patterning of nonlinear frequency conversion with transversely varying quasi-phase-matching gratings," *Opt. Lett.* **23**, 673–675 (1998).
- <sup>3</sup>J. R. Kurtz, A. M. Schober, D. S. Hum, and A. J. Saltzman, "Nonlinear physical optics with transversely patterned quasi-phase-matching gratings," *IEEE J. Sel. Top. Quantum Electron.* **8**, 660–664 (2002).
- <sup>4</sup>T. Ellenbogen, N. Voloch-Bloch, A. Ganany-Padovicz, and A. Arie, "Nonlinear generation and manipulation of Airy beams," *Nat. Photonics* **3**, 395–398 (2009).
- <sup>5</sup>G. A. Siviloglou, J. Broky, A. Dogariu, and D. Christodoulides, "Observation of accelerating Airy beams," *Phys. Rev. Lett.* **99**, 213901 (2007).
- <sup>6</sup>A. Bahabad and A. Arie, "Generation of optical vortex beams by nonlinear wave mixing," *Opt. Express* **15**, 17619–17624 (2007).
- <sup>7</sup>A. Shapira, L. Naor, and A. Arie, "Nonlinear optical holograms for spatial and spectral shaping of light waves," *Sci. Bull.* **60**, 1403–1415 (2015).
- <sup>8</sup>Y. Ming, J. Tang, Z. X. Chen, F. Xu, L. J. Zhang, and Y. Q. Lu, "Generation of N00N state with orbital angular momentum in a twisted nonlinear photonic crystal," *IEEE J. Sel. Top. Quantum Electron.* **21**, 225–230 (2015).
- <sup>9</sup>J. Tang, Y. Ming, Z. X. Chen, W. Hu, F. Xu, and Y. Q. Lu, "Entanglement of photons with complex spatial structure in Hermite-Laguerre-Gaussian modes," *Phys. Rev. A* **94**, 012313 (2016).
- <sup>10</sup>I. Dolev, T. Ellenbogen, and A. Arie, "Switching the acceleration direction of Airy beams by a nonlinear optical process," *Opt. Lett.* **35**, 1581–1583 (2010).
- <sup>11</sup>S. M. Saltiel, D. N. Neshev, W. Krolikowski, A. Arie, O. Bang, and Y. S. Kivshar, "Multiorder nonlinear diffraction in frequency doubling processes," *Opt. Lett.* **34**, 848–850 (2009).
- <sup>12</sup>M. A. Bandres and J. C. Gutiérrez-Vega, "Ince-Gaussian beams," *Opt. Lett.* **29**, 144–146 (2004).
- <sup>13</sup>M. A. Bandres and J. C. Gutiérrez-Vega, "Ince-Gaussian modes of the paraxial wave equation and stable resonators," *J. Opt. Soc. Am. A* **21**, 873–880 (2004).
- <sup>14</sup>U. T. Schwarz, M. A. Bandres, and J. C. Gutiérrez-Vega, "Observation of Ince-Gaussian modes in stable resonators," *Opt. Lett.* **29**, 1870–1872 (2004).
- <sup>15</sup>J. B. Bentley, J. A. Davis, M. A. Bandres, and J. C. Gutiérrez-Vega, "Generation of helical Ince-Gaussian beams with a liquid-crystal display," *Opt. Lett.* **31**, 649–651 (2006).
- <sup>16</sup>M. C. Gather and S. H. Yun, "Single-cell biological lasers," *Nat. Photonics* **5**, 406–410 (2011).
- <sup>17</sup>M. Reicherter, T. Haist, E. U. Wagemann, and H. J. Tiziani, "Optical particle trapping with computer-generated holograms written on a liquid-crystal display," *Opt. Lett.* **24**, 608–610 (1999).
- <sup>18</sup>M. Krenn, R. Fickler, M. Huber, R. Lapkiewicz, and W. Plick, "Entangled singularity patterns of photons in Ince-Gauss mode," *Phys. Rev. A* **87**, 012326 (2013).
- <sup>19</sup>M. M. Fejer, G. A. Magel, D. H. Jundt, and R. L. Byer, "Quasi-phase-matched second harmonic generation: Tuning and tolerances," *IEEE J. Quantum Electron.* **28**, 2631–2654 (1992).
- <sup>20</sup>A. Kuroda, S. Kurimura, and Y. Uesu, "Domain inversion in ferroelectric MgO: LiNbO<sub>3</sub> by applying electric fields," *Appl. Phys. Lett.* **69**, 1565–1567 (1996).
- <sup>21</sup>J. J. Burch, "A computer algorithm for the synthesis of spatial frequency filters," *IEEE Proc.* **55**, 599–601 (1967).
- <sup>22</sup>W. H. Lee, "Binary computer-generated holograms," *Appl. Opt.* **18**, 3661–3669 (1979).
- <sup>23</sup>M. Yamada, N. Nada, M. Saitoh, and K. Watanabe, "1st-order quasi-phase matched LiNbO<sub>3</sub> waveguide periodically poled by applying an external-field for efficient blue 2nd-harmonic generation," *Appl. Phys. Lett.* **62**, 435–436 (1993).
- <sup>24</sup>D. A. Bryan, R. Gerson, and H. E. Tomaschke, "Increased optical damage resistance in lithium niobate," *Appl. Phys. Lett.* **44**, 847–849 (1984).
- <sup>25</sup>M. Fontana, K. Chah, M. Aillerie, R. Mouras, and P. Bourson, "Optical damage resistance in undoped LiNbO<sub>3</sub> crystals," *Opt. Mater.* **16**, 111–117 (2001).
- <sup>26</sup>L. Allen, M. W. Beijersbergen, R. J. C. Spreeuw, and J. P. Woerdman, "Orbital angular momentum of light and the transformation of Laguerre-Gaussian laser modes," *Phys. Rev. A* **45**, 8185–8189 (1992).
- <sup>27</sup>J. E. Curtis, B. A. Koss, and D. G. Grier, "Dynamic holographic optical tweezers," *Opt. Commun.* **207**, 169–175 (2002).
- <sup>28</sup>M. E. J. Friese, H. Rubinsztein-Dunlop, J. Gold, P. Hagberg, and D. Hanstorp, "Optically driven micromachine elements," *Appl. Phys. Lett.* **78**, 547–549 (2001).
- <sup>29</sup>A. Mair, A. Vaziri, G. Weihs, and A. Zeilinger, "Entanglement of the orbital angular momentum states of photons," *Nature* **412**, 313–316 (2001).
- <sup>30</sup>J. H. Lee, G. Foo, E. G. Johnson, and G. A. Swartzlander, "Experimental verification of an optical vortex coronagraph," *Phys. Rev. Lett.* **97**, 053901–053904 (2006).
- <sup>31</sup>A. Shapira, R. Shiloh, I. Juwiler, and A. Arie, "Two-dimensional nonlinear beam shaping," *Opt. Lett.* **37**, 2136–2138 (2012).
- <sup>32</sup>R. W. Boyd, *Nonlinear Optics (Third Edition)* (Academic, New York, 2009), p. 78.
- <sup>33</sup>S. M. Saltiel, Y. Sheng, N. Voloch-Bloch, D. N. Neshev, W. Krolikowski, A. Arie, K. Koynov, and Y. S. Kivshar, "Cerenkov-type second-harmonic generation in two-dimensional nonlinear photonic structures," *IEEE J. Quantum Electron.* **45**, 1465 (2009).
- <sup>34</sup>A. E. Siegman, "Analysis of laser beam quality degradation caused by quartic phase aberrations," *Appl. Opt.* **32**, 5893–5901 (1993).
- <sup>35</sup>R. Borghi and M. Santarsiero, "M<sup>2</sup> factor of Bessel-Gauss beams," *Opt. Lett.* **22**, 262–264 (1997).
- <sup>36</sup>A. Parent, M. Morin, and P. Lavigne, "Propagation of super-Gaussian field distributions," *Opt. Quantum Electron.* **24**, S1701–S1709 (1992).
- <sup>37</sup>E. M. Drège, N. G. Skinner, and D. M. Byrne, "Analytical far-field divergence angle of a truncated Gaussian beam," *Appl. Opt.* **39**, 4918–4925 (2000).